

# Towards Practical Implementation of Data and Energy Integrated Networks

HU Jie<sup>1</sup>, ZHANG Yitian<sup>2</sup>, YU Qin<sup>1</sup>, and YANG Kun<sup>2</sup>

(1. University of Electronic Science and Technology of China, Chengdu 611731, China;

2. University of Essex, Essex CO4 3SQ, UK)

## 1 Introduction

With the rapid development of the mobile internet, people become indulged in their hand-held smart devices for social networking, pictures/videos sharing and online gaming. Furthermore, regular mobile devices are all equipped with powerful CPUs and large screens. Running these intense energy consuming applications quickly drains the rechargeable battery. Charging their mobile devices every single day has become an annoying recipe in people's daily life. Moreover, cable based charging restricts positions of mobile devices. Wireless charging may provide more flexible options for the holders of various types of electronic appliances.

Currently, resonant inductive coupling and magnetic resonance coupling emerge as two flexible wireless charging options for different electronic appliances. Resonant inductive coupling based wireless charging relies on the magnetic coupling that delivers electrical energy between two coils tuned to resonate at the same frequency. This technique has already been commercialised for the small electronic appliances [1], such as mobile phones, electric toothbrushes and smart watches. The coupling coils only allow the near-field wireless power to transfer at a distance from a few millimetres to a few centimeters [2], while it is capable of achieving the power transfer efficiency as high as 56.7% when working in the frequency of 508 kHz [3]. Furthermore, resonant inductive coupling requires strict alignment of the coupling coils. A small misalignment may result in dramatic reduction of the power transfer efficiency [4]. As a result, during the charging process, the elec-

### Abstract

With the rapid development of the mobile internet and the massive deployment of the Internet of Things, mobile devices, including both the consumer electronics and the sensors, become hungrier for the energy than ever before. Conventional cable based charging largely restrict the movement of the mobile devices. Wireless charging hence emerges as an essential technique for enabling our ultimate goal of charging anytime and anywhere. By efficiently exploiting the legacy of the existing communication infrastructure, we propose a novel data and energy integrated network (DEIN) in order to realise the radio frequency (RF) based wireless charging without degrading the information transmission. In this treatise, we focus on the implementation of the DEIN in both the theoretical and practical aspects, concerning the transceiver architecture design and the rectifier circuit design. Furthermore, we also present a Wi-Fi based testbed for demonstrating the availability of the RF based wireless charging.

### Keywords

data and energy integrated network (DEIN); transceiver architecture; RF-DC converter; Wi-Fi based testbed

tronic appliances cannot be freely moved.

By contrast, magnetic resonance coupling relies on the evanescent-wave coupling to generate and transfer electrical energy between two resonators. This technique has already been widely adopted for charging the electric vehicles due to its high power transfer efficiency [5]. For example, magnetic resonance coupling is capable of achieving the power transfer efficiency as high as 90% given a distance of 0.75 m [6]. Both of its power transfer efficiency and its allowable charging distance are much higher than that of the resonant inductive coupling. However, magnetic resonance coupling still belongs to the category of the near-field wireless charging, since its power transfer efficiency dramatically reduces to 30% when the distance increases to 2.25 m [6]. Nevertheless, magnetic resonance coupling does not require strict alignment between the rechargeable device and the energy source. During the charging process, the electronic appliances are therefore able to move within the charging area [7].

Supported by the above-mentioned two classic near-field wireless charging techniques, the conventional charging cables are replaced by charging plates. Restricted by their short energy transfer distance and strict alignment requirements, a rechargeable device has to be placed on the charging plate for the energy reception [8]. It is far from our ultimate goal—

This work was supported by University of Electronic Science and Technology of China under Grant No. ZYGX2016KYQD103.

**Towards Practical Implementation of Data and Energy Integrated Networks**

HU Jie, ZHANG Yitian, YU Qin, and YANG Kun

charging anytime and anywhere. Furthermore, massive sensors will be deployed for the realisation of the Internet of Things (IoT) and smart cities. Due to the difficult replacement of the sensors in some circumstances, wireless charging is an essential technique for extending the life time of the sensors as long as possible. Obviously, the near-field wireless charging techniques is not suitable for providing power supplies for the sensors.

With the dramatic growth of the wireless communication demand, a huge number of diverse information transmitters working in the radio frequency (RF) will be deployed, especially in the densely populated urban areas. Researchers have foreseen that the transmitters may outnumber the receivers in the near future, which inspires the rise of ultra-dense networks (UDNs) [9]. Consequently, the ambient environment will be filled with plenty of RF signals. If an electronic device is capable of harvesting energy from these RF signals, it may effectively solve their energy shortage issue.

Current research mainly focuses on two techniques of seeking power supply from the RF signals. The first technique is harvesting energy from the ambient RF signals, which are propagated by TV towers [10], cellular base stations [11], Wi-Fi access points [12] and more. However, due to the hostile wireless channels, the power carried by the RF signals in air is seriously attenuated and only a small fraction of power can be harvested. As a result, this technique is mostly adopted for powering sensor networks, where the duty cycles of the sensors are very long and their communication demand is very low.

The second technique is harvesting energy from the dedicated RF signals. With the aid of dedicated RF resources spanning from spectrum domain, time domain to space domain, the hostile wireless channel attenuation can be compensated by some classic wireless communication techniques, such as orthogonal frequency division multiplexing (OFDM) [13], full-duplex [14] and multiple antennas [15]. Therefore, we may eventually achieve high efficient wireless power transfer. Furthermore, some dedicated infrastructure may also be deployed for fulfilling the users' energy demand. As a result, static power beacons [16] may be massively deployed alongside the existing cellular infrastructure. Furthermore, a vehicle carrying a power beacon [17] may also patrol around a specific area covered by a mobile network in order to power the mobile nodes within it.

However, dedicated power transfer infrastructure requires additional investment, while transmitting energy on dedicated RF channels occupies additional communication resources. These may consequently harm the wireless communication performance to some extent. In order to more efficiently exploit the existing communication infrastructure, we hope to realise the integrated data and energy transfer [18], which hence results in data and energy integrated networks (DEINs). In this treatise, we focus our attention on the physical implementation of the devices in the future DEIN. Our novel contributions are listed as follows:

- We provide a thorough tutorial on the transceiver architecture design for the devices in DEINs from both the theoretical and implementation perspectives.
- We provide a thorough tutorial on the circuit design for the essential energy reception components and we also provide the tractable analysis for the RF to direct current (DC) conversion efficiency.
- We also present a Wi-Fi based wireless power transfer system in order to demonstrate the availability of the integrated data and energy transfer.

The rest of the treatise is organised as follows. In Section 2, we elaborate on the architecture design for both of the generic transmitter and the splitter based receiver. In Section 3, we provide details of the circuit design for efficiently converting the RF signal to the DC. Furthermore, a Wi-Fi based wireless power transfer prototype is presented in Section 4, followed by the final conclusion of our treatise in Section 5.

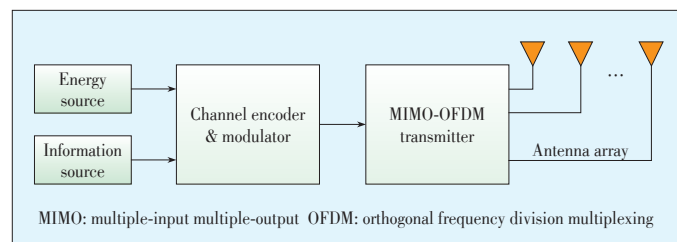
**2 Transceiver Architecture for DEIN**

In order to physically realise the simultaneous transfer of both the information and energy, we have to re-design the transceiver architecture for potential devices in DEINs, e.g. sensors, vehicles and mobile handsets.

**2.1 Transmitter Architecture**

The transmitter architecture of devices in DEINs is not quite different from their current commercialised counterparts designed for data transmission, as illustrated in **Fig. 1**. A typical transmitter in DEINs consists of several important components.

After responding to an information requester, the application layer of the transmitter, which is regarded as the “information source” in Fig. 1, generates a sequence of the information bits and pushes these bits into the channel encoder as well as the modulator. Some of the redundant bits are added to the original information bits in order to enhance the communication reliability before being modulated to the pass band for transmission. Note that all the energy required for this signal processing comes from the energy source of the transmitter. For example, additional redundant bits may consume extra energy in order to form additional signal waves and the modulator may also consume energy in order to modulate the information by the pulse-amplitude, which is well known as the pulse-amplitude modulation (PAM). As a result, after the channel encod-



▲ **Figure 1. The transmitter architecture of devices in DEINs.**

er and the modulator, the pass-band signal waves carry both the information and the energy. A careful design of the channel encoder as well as the modulator may substantially improve the performance of the simultaneous information and energy transfer.

Additionally, the transmitter in Fig. 1 is also capable of responding to an energy requester. After receiving the request from an energy receiver, the information source of the transmitter may generate a sequence of dummy bits in order to carry the requested energy.

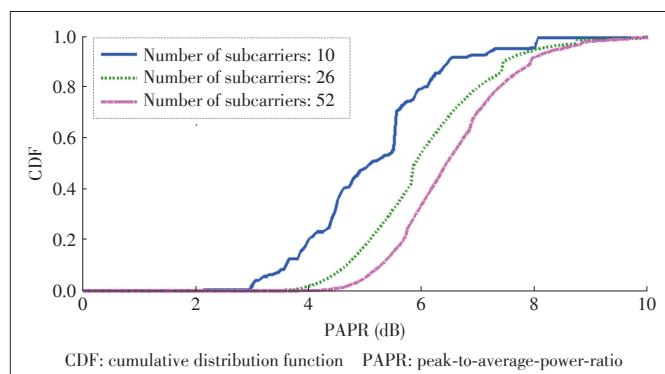
Either the dummy bits for pure energy transfer or the information bits for simultaneous information and energy transfer may be modulated into the transmit symbols and further flow into the multiple-input multiple-output (MIMO) and the OFDM module. MIMO technique may provide a range of benefits for both the information and energy transfer as follows:

- Independent spatial channels provide diversity gains for enhancing the reliability of the information transmission [19] and for strengthening the energy transfer [20].
- Independent spatial channels provide multiplexing gains for increasing the throughput of the information transmission [21] as well as providing additional tunnels for dedicated energy transfer [22].
- With the aid of multiple transmit antennas, the transmitter is allowed to focus the main lobe of its beam towards the receiver for the sake of counteracting the channel attenuation [23]. This is even crucial for the wireless energy transfer since the energy reception efficiency is very sensitive to the received power level [24].

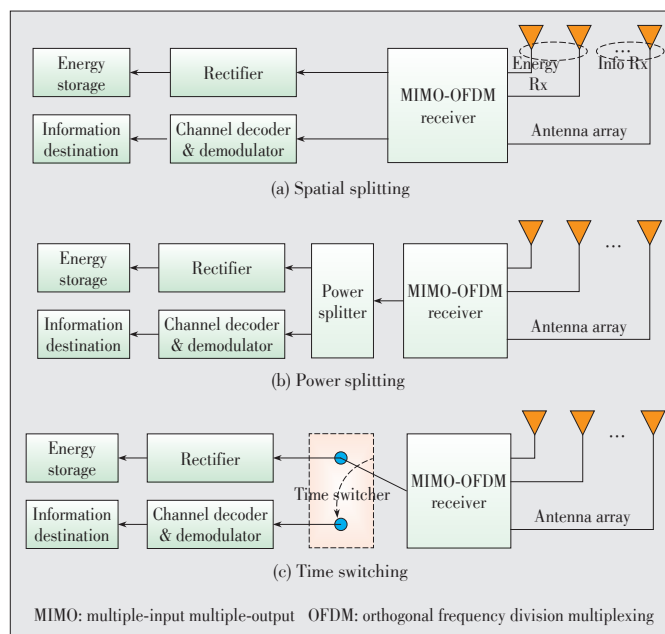
Furthermore, OFDM is another important technique for the transmitter in DEINs. A higher received power level may better stimulate the energy reception circuit and hence increase the RF-DC conversion efficiency. We plot the cumulative distribution function (CDF) of the peak-to-average-power-ratio (PAPR) of a 802.11a based OFDM system associated with the binary-phase-shift-keying (BPSK) modulation in Fig. 2. We observe from Fig. 2 that if a higher number of subcarriers are allocated to a transmitter-receiver pair, the PAPR is substantially increased. Fig. 2 demonstrated that OFDM is capable of providing a waveform of high PAPR, which may remarkably increase the energy delivery efficiency.

## 2.2 Splitter Based Receiver Architecture

Let us now investigate the receiver architecture design of devices in DEINs. Fig. 3 illustrates three splitter based receiver architectures, in which the signal is split in spatial, power and time domains, respectively. Apart from different signal splitting approaches, these three receiver architectures share the other components in common. After being received by the MIMO-OFDM receiver, the RF signal is split into two parallel flows. One is for energy reception, where the rectifier plays an important role in converting the RF signal to the DC before it can be stored in the receiver's battery. The other is for conven-



▲ Figure 2. The CDF of the PAPR of a 802.11a based OFDM system associated with the BPSK modulation. The size of the Fast-Fourier-Transformation (FFT) is 128. The maximum number of subcarriers is 52.



▲ Figure 3. Three signal splitting based receiver architecture for devices in DEINs: (a) Spatial splitting based receiver architecture; (b) Power splitting based receiver architecture; and (c) Time switching based receiver architecture.

tional information reception, where the RF signal is transformed from the pass band to the base band for further demodulation and decoding operations before it arrives at the information destination. Due to the signal splitting operation, the tradeoff between the energy reception and the information reception clearly exists. An optimal signal splitting approach in order to serve different purposes is crucial for the design of a splitter based receiver architecture. Next, we will study the implementation of three typical splitting approaches, namely the spatial splitting (SS), the power splitting (PS) and the time switching (TS). Without loss of generality, the splitting factor is denoted as  $\rho$  ( $0 \leq \rho \leq 1$ ), which indicates that a portion  $\rho$  of the RF signal will be invoked for delivering the energy and

the rest  $(1-\rho)$  of the RF signal will be invoked for delivering the information.

In the SS based receiver, as shown in Fig. 3a, the signal is split by allocating different number of antennas at the receiver for the energy and information receptions, respectively. For the implementation of the SS based receiver, we have to jointly optimise the antenna selection on the receiver side as well as the transmit power allocation on the transmitter side so as to achieve the maximum information rate subject to the requirement of the energy reception. For example, in [25], by invoking an antenna selection scheme and the interference alignment technique, the authors partitioned the received signal into two orthogonal spaces in order to achieve simultaneous information and energy transfer. In [26], the problem was formulated as a joint optimisation of both the antenna selection and the transmit covariance matrix design in order to achieve the maximum information rate subject to the energy harvesting constraint.

In the PS based receiver, the signal is split by the power splitters for realising the independent energy and information receptions, as illustrated in Fig. 3b. With the aid of the MIMO system, we can realise the transmission of several independent information flows and hence substantially increase the information throughput. In order to extract energy from these independent information flows, each receive antenna should be equipped with a power splitter. These power splitters are capable of adaptively tuning themselves to conceive specific splitting factors. As a result, for the implementation of the PS based receiver, we have to jointly optimise the splitting factors for each antenna on the receiver side as well as the transmit power allocation on the transmitter side so as to achieve the balance between the information rate and the energy reception. For example, the authors of [27] focused their attention on the impact of channel estimation on the performance of integrated data and energy transfer by jointly designing the PS factor as well as the duration of both the training phase and the transmission phase. Furthermore, the authors of [28] extended the point-to-point scenario to a multi-relay cooperative network. They proposed a harvest-use-store PS relaying strategy with distributed beamforming for wireless-powered multi-relay cooperative networks.

Furthermore, several existing works focus on the circuit design for a practical power splitter of high performance. For example, the authors of [29] proposed a 1-V wideband CMOS phase and power splitter (PPS) with an RLC network load and frequency compensation capacitor. This power splitter could only produce 7 degree error for phase and 1.4 dB power imbalance. The authors of [30] presented a V-band active one-to-four power splitter in 90-nm LP CMOS process for phased-array transmitter. In their power splitter, 0.75 dB power imbalance and 4.3 degree phase error were achieved.

In the TS based receiver, the signal is split in the time domain by a time switcher for the independent energy and information receptions, as illustrated in Fig. 3c. For its practical im-

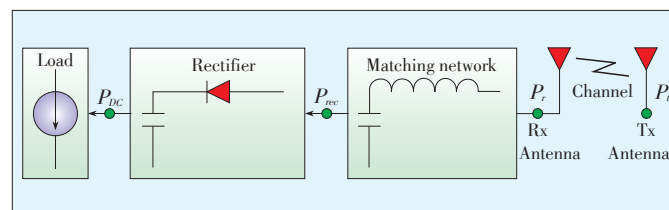
plementation, we only need to partition a typical transmission frame into two parts, namely the energy transfer sub-frame and the information transfer sub-frame dedicated for the energy and information receptions respectively. However, having diverse TS factors for each antenna is not quite realistic since this operation may result in the mismatch of the RF signals received by the independent channels, which may significantly complicate the subsequent signal and energy processing. As a result, all the antennas on the receiver side are assumed to have identical TS factors. Therefore, for the implementation of the TS based receiver, we have to jointly optimise both the power allocation on the transmitter side and the TS factors on the receiver side in order to achieve the balance between the information rate and the energy reception. For example, the authors of [31] studied the tradeoff between the energy consumption and the transmission delay by proposing a dynamic algorithm for optimally allocating the transmit power and deciding the TS factor. In [32], the authors maximised the end-to-end achievable information rate in the decode-and-forward relay network by jointly optimising both the transmit power and the TS factor.

### 3 Converting Radio-Frequency Signal to Direct-Current

As shown in Fig. 3, rectifiers play essential roles in the integrated data and energy reception. An efficient rectifier is capable of converting a remarkable portion of the received RF signal into the DC so as to boost the performance of wireless charging. Besides focusing on the rectifier itself, we will consider the overall energy conversion efficiency from the transmitter side to the receiver side.

#### 3.1 Overall Energy Conversion Efficiency

As shown in Fig. 4, we consider an overall energy converter for the wireless energy transfer. The RF signal amplified by the power  $P_t$  is transmitted by the antenna on the transmitter side. After being attenuated by the wireless channel, the power of the received RF signal is only  $P_r$ . We can simply formulate the relationship between  $P_t$  and  $P_r$  as  $P_r = \eta_w P_t$ , where the energy conversion efficiency  $\eta_w$  is determined by various types of wireless channel attenuation. Then, the RF signal flows into the matching network first in order to alleviate the impedance changes between the receive antenna and the rectifier. However, the matching network results in inevitable energy loss. The relationship between the input power  $P_r$  of the



▲ Figure 4. An overall energy converter for the wireless energy transfer.

RF signal to the matching network and the resultant output power  $P_{rec}$  is simply formulated as  $P_{rec} = \eta_{mn} P_r$ , where the conversion efficiency  $\eta_{mn}$  is determined by the topology and the electronic components of the matching network. Finally, the RF signal goes to the rectifier. The converted power of the DC signal is  $P_{DC} = \eta_{rec} P_{rec}$ , where  $\eta_{rec}$  is the conversion efficiency of the rectifier. As a result, the relationship between the transmit power  $P_t$  and the final DC power  $P_{DC}$  can be formulated as

$$P_{DC} = \eta_w \cdot \eta_{mn} \cdot \eta_{rec} \cdot P_t, \quad (1)$$

where  $\eta_{mn} \cdot \eta_{rec}$  is the conversion efficiency  $\eta_E$  from the received RF power  $P_r$  to the DC power  $P_{DC}$  as commonly assumed in the literature.

### 3.2 RF Propagation and Aperture Antenna

The first component of the overall energy transfer system is the wireless channel. The generic form of the path loss for the RF propagation is formulated as:

$$\eta_{pl} = G_t \cdot G_r \cdot \left( \frac{c}{4\pi f d_0} \right)^2 \cdot \left( \frac{d_0}{d} \right)^\alpha, \quad (2)$$

where  $G_t$  and  $G_r$  are the transmit and receive antenna gains, respectively, while  $c$  is the speed of the light,  $f$  is the carrier frequency, and  $\alpha$  is the path loss exponent. Furthermore,  $d_0$  and  $d$  are the reference distance and the actual signal radiation distance, respectively. Specifically, when  $\alpha = 2$ , (2) becomes the well-known Friis' law for free-space radio propagation. Generally, the path loss exponent  $\alpha$  is between 2 and 6, depending on a specific propagation scenario. For an indoor scenario, where  $d_0 = 1$  m,  $d = 10$  m,  $\alpha = 3$ ,  $f = 2.4$  GHz, when isotropic transmit and receive antennas are conceived, namely  $G_t = G_r = 1$ ,  $\eta_{pl}$  is  $-70$  dB according to (2),  $\eta_{pl}$  is further degraded by increasing the carrier frequency  $f$ . For example, in IEEE 802.11ad, which works in 60 GHz millimetre wave (mmWave),  $\eta_{pl}$  is as low as  $-98$  dB at the same distance of  $d = 10$  m. Apart from the serious path loss, the RF signal is further attenuated by the multipath fading. The conversion efficiency  $\eta_{mul}$  is the power of the multipath fading amplitude. When the RF propagation distance is short, a line-of-sight path always exists between the transmitter and receiver. In this case, the multipath fading may be reasonably modelled as a Rice distribution. Hence, the energy conversion efficiency of the wireless channel can be expressed as  $\eta_w = \eta_{pl} \cdot \eta_{mul}$ .

The energy reception and information reception circuits have different levels of sensitivity for the received power  $P_r$ . For example, the effective received power level  $P_r$  is in the order of  $-80$  dBm for successful information recovery, thanks to the implementation of the advanced error correction techniques. By contrast, the effective received power level  $P_r$  for triggering the energy reception circuit is in the order of  $-10$

dB, much higher than its information reception counterpart. In order to guarantee the effective energy transfer, aperture antenna is capable of compensating the tremendous energy loss during the signal propagation, due to its high directivity. For the free space radio propagation scenario, we can rewrite  $\eta_{pl}$  in the following equation [33]:

$$\eta_{pl} = \frac{A_{eff,t} \cdot A_{eff,r}^2}{\lambda^2} \cdot \frac{1}{d^2}, \quad (3)$$

where  $A_{eff,t}$  and  $A_{eff,r}$  are the aperture areas for the transmit antenna and receive antenna respectively, while  $\lambda$  is the wavelength of the radio signal. The aperture area of the isotropic antenna is  $A_{eff}^{iso} = \lambda^2/4\pi$ . Hence, given the unity gain of the isotropic antenna, the gain of a directional antenna having an aperture area of  $A_{eff}$  is expressed as  $G_t = 4\pi A_{eff}/\lambda^2$ . Compared to the isotropic antenna based path loss of (2), the aperture antenna based path loss of (3) presents inverse trend with respect to the carrier frequency. For example, a beam at 80 GHz will have about 30 dB gain (narrower beam) compared to the beam at 2.4 GHz frequency if the antenna areas are kept constant.

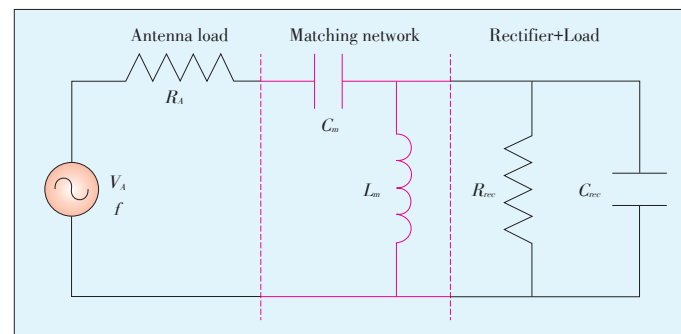
### 3.3 Matching Network

As explained in Section 3.2, after being attenuated by the hostile wireless channel, the received RF signal has a very low amplitude. There is not any margin to lose for transferring the RF signal of low amplitude from the antenna to the rectifier. As a result, we have to carefully design a circuit for matching the impedance of the antenna to that of the rectifier. This circuit is regarded as a matching network.

Fig. 5 illustrates a typical L-match topology based circuit for the impedance match. In this example, the antenna is roughly modelled by an alternative-current (AC) voltage  $V_A$  working in the carrier frequency  $f$  of the RF signal and a resistance  $R_A$ . The amplitude of  $V_A$  generated by the antenna is given by [34]

$$V_A = 2 \cdot \sqrt{2R_A P_r}, \quad (4)$$

where  $P_r$  is the RF signal power received by the antenna as shown in Fig. 4. The rectifier and the ensuing load are jointly



▲ Figure 5. A typical L-match topology based matching network.

modelled by a resistance  $R_{rec}$  and a capacitor  $C_{rec}$  in parallel [35].

As shown in Fig. 5, the L-match topology comprises of a capacitor  $C_m$  and an inductor  $L_m$ . Note that  $C_m$  is connected to  $R_{rec}$  and  $C_{rec}$  sequentially but  $L_m$  is connected to them in parallel. The values of  $C_m$  and  $L_m$  are given by

$$C_m = \frac{1}{\omega R_A} \cdot \frac{R_A}{\sqrt{R_{rec} - R_A}}, \quad (5)$$

$$L_m = \frac{R_{rec}}{\omega} \cdot \frac{1}{\omega R_{rec} C_{rec} + 1 / \sqrt{\frac{R_A}{R_{rec} - R_A}}}, \quad (6)$$

where  $\omega = 2\pi f$  is the angular frequency of the received RF signal.

The voltage gain of the L-match topology is expressed as

$$G = \frac{V_{rec}}{V_A} = \frac{1}{2} \cdot \frac{\sqrt{R_{rec}}}{\sqrt{R_A}}. \quad (7)$$

According to (7), for  $R_{rec} > R_A$ , the voltage can be effectively boosted by the L-match topology. Furthermore, the power conversion efficiency of the matching network can be expressed as

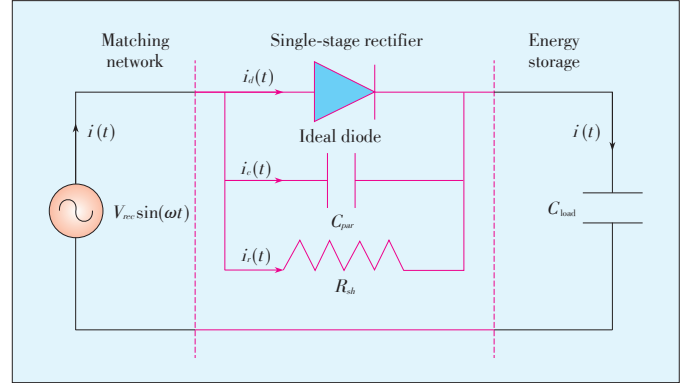
$$\eta_{mn} = G^2 = \frac{1}{4} \frac{R_{rec}}{R_A}. \quad (8)$$

In order to maximise the power conversion efficiency of the L-match topology, the following procedure has to be carried out. A proper voltage gain should be selected and the resistance  $R_{rec}$  can be determined according to (7) by assuming a given value for  $R_A$ . Finally, given  $\omega$  and  $C_{rec}$ , the values of the components in the L-match topology can be derived by (5) and (6). Note that the L-match topology of Fig. 5 is a high-pass matching network. If we exchange the position of  $L_m$  and that of  $R_m$ , we obtain a low-pass matching network. Furthermore, a multi-stage L-match topology is also proposed in [36]. Due to its simplicity, the L-match topology is widely adopted in the circuit design of the RF energy reception. Interested readers may refer to [37]–[39] for more technical details.

### 3.4 Rectifier Design

After the impedance matching, the RF-signal flows into the rectifier in order to be converted into the DC signal. The rectifier is an essential component for the energy reception in the receiver architecture of Fig. 3.

Fig. 6 shows a single stage rectifier, which comprises of an ideal diode, a parasitic capacitor  $C_{par}$  and a resistor  $R_{sh}$ . The input AC voltage  $V_{rec} \sin(\omega t)$  of the rectifier is the output one from the matching network, where  $\omega = 2\pi f$  is the angular frequency of the received RF signal. The amplitude of  $V_{rec}$  can be obtained with the aid of (7), if the L-match topology is invoked.



▲ Figure 6. A single stage rectifier for converting the RF signal into the DC.

The energy storage unit is a capacitor  $C_{load}$  as an example.

The current  $i_d(t)$  flowing through an ideal diode with an AC voltage  $v_d(t)$  is expressed as [40]

$$i_d(t) = I_s \cdot e^{\frac{v_d(t)}{M V_T} - 1}, \quad (9)$$

where  $I_s$  is the saturation current,  $V_T$  is the thermal voltage and  $M$  is the ideal factor. The value of the parasitic capacitor  $C_{par}(t)$  depends on the voltage  $v_d(t)$ , which can be expressed as

$$C_{par}(t) = C_0 \left( 1 - \frac{v_d(t)}{V_0} \right)^{-\frac{1}{2}}, \quad (10)$$

where  $C_0$  is the zero bias junction capacitance and  $V_0$  is a constant having a typical value of 0.6 V to 0.8 V. The current  $i_c(t)$  through  $C_{par}(t)$  is derived as

$$i_c(t) = \frac{d(C_{par}(t)v_d(t))}{dt} = C_{par}(t) \frac{dv_d(t)}{dt} + v_d(t) \frac{dC_{par}(t)}{dt}. \quad (11)$$

Furthermore, the current flowing through the resistor  $R_{sh}$  is expressed as  $i_r(t) = v_d(t)/R_{sh}$ . Finally, we have  $i(t) = i_d(t) + i_c(t) + i_r(t)$ . The net electric charge accumulated at the energy storage capacitance during a single charging cycle  $T$  is derived as

$$\Delta Q = \int_0^T i_d(t) dt + \int_0^T i_c(t) dt + \int_0^T i_r(t) dt, \quad (12)$$

where  $T = 1/f$ . For simplicity, the authors of [0] assume  $R_{sh} = +\infty$  and hence we have  $i_r(t) = 0$ . Furthermore, we also have  $v_d(t) = V_{rec} \sin(\omega t) - V_c$ , where  $V_c$  is the voltage of the energy storage capacitance, which remains constant during a charging cycle  $T$ .

The periodic property of the sinusoidal wave results in the symmetric nature of  $i_c(t)$  over a charging cycle  $T$  and hence the corresponding integral  $\int_0^T i_c(t) dt$  is equal to zero. Eventually the net electric charge  $\Delta Q$  only depends on  $i_d(t)$ , which

can be further derived as

$$\Delta Q = \int_0^T i_d(t) dt = \int_0^T I_s \cdot \left( e^{\frac{v_d(t)}{MV_T} - 1} \right) dt = I_s T \left[ e^{-\frac{V_c}{MV_T}} \mathcal{F}_0 \left( \frac{V_{rec}}{MV_T} \right) \right], \quad (13)$$

where  $\mathcal{F}_0(\cdot)$  is the modified Bessel function of first kind and having an order of zero. In the steady state, the electric charge flowing into the load  $C_{load}$  should be equal to that leaving the load, which indicates  $\Delta Q = 0$ . According to this fact, we can derive the voltage  $V_c$  of the energy storage capacitance, which is expressed as

$$V_c = MV_T \cdot \log \left[ \mathcal{F}_0 \left( \frac{V_{rec}}{V_T} \right) \right]. \quad (14)$$

Furthermore, the power conversion efficiency of the rectifier is expressed as

$$\eta_{rec} = \left( \frac{V_c}{V_{rec}} \right)^2 = \left( \frac{MV_T}{V_{rec}} \log \left[ \mathcal{F}_0 \left( \frac{V_{rec}}{V_T} \right) \right] \right)^2 \quad (15)$$

Normally, connected multi-stage rectifiers having the same capacitors and diodes are practically implemented for harvesting energy from the RF signal [41], [42]. Fortunately, the performance of the multi-stage rectifiers can be well approximated by the above-introduced single-stage rectifier [43].

After characterising the power conversion efficiency for every component in Fig. 4, we finally obtain a practical expression for the power conversion efficiency of the overall system, which is expressed as  $\eta_w \cdot \eta_{mn} \cdot \eta_{rec}$ .

### 3.5 Energy Storage

Thanks to the above-mentioned physical implementation, the energy harvested from the RF signal now is able to drive the electric load or to be stored in the energy storage unit. There are two typical energy storage units for different application scenarios.

The first one is the capacitor based energy storage, such as the load capacitor  $C_{load}$  in Fig. 6, where the energy is stored in the electric field between its insulated plate. The two equations in (16) characterise the discharging and the charging processes of a capacitor respectively [44]:

$$Q(t) = Q_0 e^{-\frac{t}{RC}}, \quad Q(t) = Q_0 \left( 1 - e^{-\frac{t}{RC}} \right), \quad (16)$$

where  $Q(t)$  is the charge remained in the capacitor at time  $t$ ,  $Q_0$  is the maximum charge that the capacitor can store,  $R$  is the affiliated resistance and  $C$  is the capacitance of the capacitor. According to these two equations, we observe that as an energy storage unit, the capacitor has a very fast charging and discharging rate. Furthermore, due to its distinct energy storage mechanism, it has unlimited rechargeable life cycles. How-

ever, the capacitor also has some obvious drawbacks as an energy storage unit. For example, it is only capable of storing a small amount of energy in its electric field and its energy leakage is significant. Furthermore, during the discharging process, the capacitor cannot provide a stable voltage since its voltage  $v(t)$  linearly depends on the amount of the charge, namely  $Q(t) = C \cdot v(t)$ . According to this distinct nature, capacitors are suitable to be implemented in sensors for collecting energy and powering their sensing cycles [45], [46]. Since sensors work with very low power consumption, they have a long duty cycle and it is difficult to frequently replace their energy storage units.

The second one is the rechargeable battery based energy storage, such as Lithium-ion (Li-ion) and Nickel Metal Hydride (NiMH) batteries. These batteries store energy by chemicals residing in it. Hence, the energy storage of rechargeable batteries is more stable than that of capacitors. According to [47], the state  $Q(t)$  of the charge at time  $t \geq t_0$  in the rechargeable battery system is expressed as

$$Q(t) = \begin{cases} \int_{t_0}^t \gamma(\tau) [i_r(\tau) - i_l(\tau)] d\tau + Q(t_0), & Q(t) \leq Q_{\max}(t), \\ Q_{\max}(t), & \text{otherwise} \end{cases} \quad (17)$$

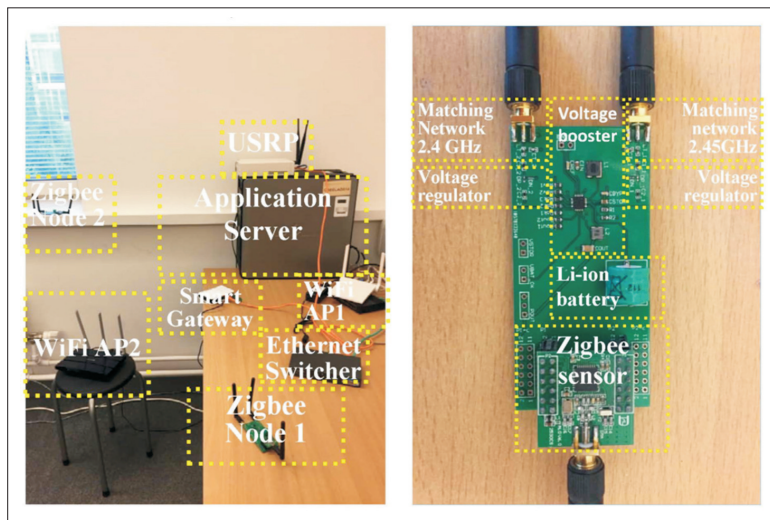
where  $i_r(t)$  is the rechargeable current at time  $t$ ,  $i_l(t)$  is the current demanded by the load and  $Q_{\max}(t)$  is the potential maximum charge at time  $t$ . In particular, the function  $\gamma(t)$  in (17) represents the recharging efficiency. Generally speaking, the function  $\gamma(t)$  approaches to zero as the charge of the battery gets close to its maximum  $Q_{\max}(t)$ . By contrast, at a lower charge level,  $\gamma(t)$  is close to a unity. Note that when the recharging current  $i_r(t)$  is higher than the required current  $i_l(t)$ , (17) illustrates a charging process. By contrast, when  $i_r(t) < i_l(t)$ , (17) characterises a discharging process. Furthermore, the energy leakage (self-discharge) of rechargeable batteries is remarkably smaller than that of capacitors. For example, the discharge of a Li-ion battery in a month, is only 2%–3% of its total amount of charge. Rechargeable batteries may also provide constant voltage during the discharging process. According to these distinctive characteristics, rechargeable batteries are widely implemented for providing stable power for the mobile consumer electronic devices, such as smart phones, tablets and laptops. Fulfilling both the information and energy demand of these devices is the prime goal of DEINs [48], [49].

## 4 A Wi-Fi Based Testbed

As shown in Fig. 7a, our Wi-Fi based testbed for the energy transfer experiment consists of two Zigbee nodes, two Wi-Fi access points (APs), a smart-gateway, a Universal Software Radio Peripheral (USRP) and a central server as well as an Ethernet switcher. A rechargeable Zigbee node comprises of a wireless energy reception circuit board and a Zigbee sensor board (Fig.

## Towards Practical Implementation of Data and Energy Integrated Networks

HU Jie, ZHANG Yitian, YU Qin, and YANG Kun



▲ Figure 7. A prototype of the DEIN: (a) A Wi-Fi based testbed; and (b) A Zigbee node.

7b). The Wi-Fi APs are invoked for providing wireless connection to the Zigbee nodes and for transferring energy to them. The smart gateway is deployed for the basic control signalling exchange as well as for collecting the sensing data uploaded by the Zigbee nodes. The USRP is implemented for detecting the conditions of the Wi-Fi channels, while the central server is for coordinating the data and energy transfer of the Wi-Fi APs. Except the Zigbee nodes, all the other components in our testbed are connected by the Ethernet switcher.

Our wireless energy reception circuit installed in a rechargeable Zigbee node has the following components: two matching networks, a voltage regulator and a voltage booster (Fig. 7b). Two sets of the L-match topology are adopted for the impedance matching at the frequencies of 2.4 GHz and 2.45 GHz, respectively. These two bands are capable of covering almost all possible Wi-Fi channels. The negative amplitude of the waveform of the received RF signal is reversed by two diodes implemented in the voltage regulator. A programmable chip bq25570, supplied by Texas Instruments, operates as the voltage booster in our wireless energy reception circuit. The converted DC voltage is used for charging a Li-ion battery. In our testbed, we program the chip bq25570 to supply the continuous DC until the voltage of the battery reaches 3.6 V. The chip may resume to work again when the battery voltage falls below 2 V. The Zigbee chip CC2530 is programmed to carry out sensing duties.

Apart from its regular sensing duties, the Zigbee chip CC2530 also monitors the voltage level of its own rechargeable battery in every five minutes. Once the voltage falls below 2 V, the Zigbee node sends the charging request to the smart gateway. The request is forwarded to the central server by the smart gateway. Together with the information of the channel state conditions offered by the USRP, the central server may schedule an optimal Wi-Fi AP for fulfilling the charging re-

quest of the Zigbee node without degrading the communication performance of other nodes in the network.

In our testbed, the energy transmitter is implemented in the Wi-Fi APs. An executable program is installed at the APs in order to realise the function of wireless energy transfer. When a Wi-Fi AP is instructed by the central server to transfer the energy to a requester, it may first create a socket of the User Datagram Protocol (UDP). Then a UDP based energy packet having a high energy density spectrum is constructed. Afterwards, the isotropic antenna of the Wi-Fi AP continuously broadcasts copies of this energy packet until the battery of the target Zigbee is full of charge. Furthermore, multiple Wi-Fi APs, operating in different bands, may be sequentially coordinated by the central server in order to cooperatively transfer the energy to the target Zigbee node.

The RF based wireless charging testbed has attracted tremendous interest from the electronic and communication engineers. The authors of [50] incorporated the ultra-wideband retro-reflective beamforming technique into the wireless charging system. In this system, at the energy transmitter, the antennas are capable of forming a direction beam towards the energy receiver, as introduced in Section 3.2. The authors of [51] invented a RF based wireless charging system for wireless sensor network (WSN). Their testbed consists of multiple sensors equipped with dedicated energy reception modules, a Powercast TX91501 as an energy transmitter, and a Zigbee coordinator working as both a sink and a synchroniser. In their system, all the sensors are equipped with rechargeable batteries. These batteries keep requesting the energy from the energy transmitter.

Different from the testbeds constructed in [50] and [51], our system has a relatively simple hardware structure. An energy reception circuit board is embedded in a Zigbee based sensor. The charging process in our system works in an on-demand mode, which may reduce the adverse effect of the wireless charging on the other communication pairs in the same network. Our system is capable of achieving the harmonious coordination between the data transmission and energy transmission, which is the prime goal of DEINs.

## 5 Conclusions

Due to the massive usage of mobile devices, charging anytime and anywhere becomes as essential as communicating anytime and anywhere, which inspires a promising prospect for the deployment of DEINs. However, the actual deployment of DEINs is not even widely tested in the lab and it is far from practice. As a result, this treatise aims for pushing the concept of DEINs a step closer towards its practical deployment. To this end, we provide a thorough tutorial on the transceiver and the circuit design for the integrated data and energy transfer.

At last, we present our testbed based on harvesting the RF signal from the Wi-Fi access point so as to demonstrate the availability of the potential deployment of DEINs.

#### References

- [1] P. S. Riehl, A. Satyamoorthy, H. Akram, et al., "Wireless power systems for mobile devices supporting inductive and resonant operating modes," *IEEE Transactions on Microwave Theory and Techniques*, vol. 63, no. 3, pp. 780–790, Mar. 2015. doi: 10.1109/WPT.2014.6839626.
- [2] M. Pinuela, D. C. Yates, S. Lucyszyn, and P. D. Mitcheson, "Maximizing DC-to-load efficiency for inductive power transfer," *IEEE Transactions on Power Electronics*, vol. 28, no. 5, pp. 2437–2447, May 2013. doi: 10.1109/TPEL.2012.2215887.
- [3] H. Liu. (2011). *Maximizing efficiency of wireless power transfer with resonant inductive coupling* [Online]. Available: [http://hxl95.github.io/media/ib\\_ee.pdf](http://hxl95.github.io/media/ib_ee.pdf)
- [4] C. Zheng, H. Ma, J. S. Lai, and L. Zhang, "Design considerations to reduce gap variation and misalignment effects for the inductive power transfer system," *IEEE Transactions on Power Electronics*, vol. 30, no. 11, pp. 6108–6119, Nov. 2015.
- [5] J. M. Miller, O. C. Onar, and M. Chinthavali, "Primary-side power flow control of wireless power transfer for electric vehicle charging," *IEEE Journal of Emerging and Selected Topics in Power Electronics*, vol. 3, no. 1, pp. 147–162, Mar. 2015. doi: 10.1109/JESTPE.2014.2382569.
- [6] A. Kurs, A. Karalis, R. Moffatt, J. D. Joannopoulos, P. Fisher, and M. Soljacic, "Wireless power transfer via strongly coupled magnetic resonances," *Science*, vol. 317, no. 5834, pp. 83–86, 2007. doi: 10.1126/science.1143254.
- [7] H. Hwang, J. Moon, B. Lee, C. h. Jeong, and S. w. Kim, "An analysis of magnetic resonance coupling effects on wireless power transfer by coil inductance and placement," *IEEE Transactions on Consumer Electronics*, vol. 60, no. 2, pp. 203–209, May 2014. doi: 10.1109/TCE.2014.6851995.
- [8] C. Y. Liou, C. J. Kuo, and S. G. Mao, "Wireless power transfer system using near-field capacitively coupled resonators," *IEEE Transactions on Circuits and Systems II: Express Briefs*, vol. PP, no. 99, pp. 1–1, 2016.
- [9] A. Gotsis, S. Stefanatos, and A. Alexiou, "Ultradense networks: the new wireless frontier for enabling 5G access," *IEEE Vehicular Technology Magazine*, vol. 11, no. 2, pp. 71–78, June 2016. doi: 10.1109/MVT.2015.2464831.
- [10] R. J. Vyas, B. B. Cook, Y. Kawahara, and M. M. Tentzeris, "E-WHEP: a batteryless embedded sensor-platform wirelessly powered from ambient digital-TV signals," *IEEE Transactions on Microwave Theory and Techniques*, vol. 61, no. 6, pp. 2491–2505, Jun. 2013. doi: 10.1109/TMTT.2013.2258168.
- [11] A. H. Sakr and E. Hossain, "Analysis of k-tier uplink cellular networks with ambient RF energy harvesting," *IEEE Journal on Selected Areas in Communications*, vol. 33, no. 10, pp. 2226–2238, October 2015. doi: 10.1109/JSAC.2015.2435358.
- [12] U. Olgun, C. c. Chen, and J. L. Volakis, "Design of an efficient ambient Wi-Fi energy harvesting system," *IET Microwaves, Antennas Propagation*, vol. 6, no. 11, pp. 1200–1206, Aug. 2012. doi: 10.1049/iet-map.2012.0129.
- [13] S. Yin and Z. Qu, "Resource allocation in multiuser OFDM systems with wireless information and power transfer," *IEEE Communications Letters*, vol. 20, no. 3, pp. 594–597, Mar. 2016.
- [14] X. Kang, C. K. Ho, and S. Sun, "Full-duplex wireless-powered communication network with wireless causality," *IEEE Transactions on Wireless Communications*, vol. 14, no. 10, pp. 5539–5551, Oct. 2015. doi: 10.1109/TWC.2015.2439673.
- [15] X. Chen, X. Wang, and X. Chen, "Energy-efficient optimization for wireless information and power transfer in large-scale MIMO systems employing energy beamforming," *IEEE Wireless Communications Letters*, vol. 2, no. 6, pp. 667–670, Dec. 2013.
- [16] Y. Ma, H. Chen, Z. Lin, Y. Li, and B. Vucetic, "Distributed and optimal resource allocation for power beacon-assisted wireless-powered communications," *IEEE Transactions on Communications*, vol. 63, no. 10, pp. 3569–3583, Oct. 2015. doi: 10.1109/TCOMM.2015.2468215.
- [17] S. W. Ko, S. M. Yu, and S. L. Kim, "The capacity of energy-constrained mobile networks with wireless power transfer," *IEEE Communications Letters*, vol. 17, no. 3, pp. 529–532, Mar. 2013. doi: 10.1109/LCOMM.2013.020413.122729.
- [18] K. Yang, Q. Yu, S. Leng, B. Fan, and F. Wu, "Data and energy integrated communication networks for wireless big data," *IEEE Access*, vol. 4, pp. 713–723, 2016.
- [19] B. S. Chen, K. C. J. Lin, S. L. Chiu, R. Lee, and H. Y. Wei, "Multiplexing-diversity medium access for multi-user MIMO networks," *IEEE Transactions on Mobile Computing*, vol. 15, no. 5, pp. 1211–1223, May 2016. doi: 10.1109/TMC.2015.2450744.
- [20] Y. Zeng and R. Zhang, "Optimized training for net energy maximization in multi-antenna wireless energy transfer over frequency-selective channel," *IEEE Transactions on Communications*, vol. 63, no. 6, pp. 2360–2373, Jun. 2015. doi: 10.1109/TCOMM.2015.2424420.
- [21] A. Stavridis, M. D. Renzo, and H. Haas, "Performance analysis of multistream receive spatial modulation in the MIMO broadcast channel," *IEEE Transactions on Wireless Communications*, vol. 15, no. 3, pp. 1808–1820, Mar. 2016. doi: 10.1109/WCOM.2015.2424420.
- [22] S. Timotheou, I. Krikidis, S. Karachontzitis, and K. Berberidis, "Spatial domain simultaneous information and power transfer for MIMO channels," *IEEE Transactions on Wireless Communications*, vol. 14, no. 8, pp. 4115–4128, Aug. 2015. doi: 10.1109/TWC.2015.2416721.
- [23] Y. Li and V. Jandhyala, "Design of retrodirective antenna arrays for short-range wireless power transmission," *IEEE Transactions on Antennas and Propagation*, vol. 60, no. 1, pp. 206–211, Jan. 2012. doi: 10.1109/TAP.2011.2167897.
- [24] V. Kuhn, C. Lahuec, F. Seguin, and C. Person, "A multi-band stacked RF energy harvester with RF-to-DC efficiency up to 84%," *IEEE Transactions on Microwave Theory and Techniques*, vol. 63, no. 5, pp. 1768–1778, May 2015. doi: 10.1109/TMTT.2015.2416233.
- [25] B. Koo and D. Park, "Interference alignment and wireless energy transfer via antenna selection," *IEEE Communications Letters*, vol. 18, no. 4, pp. 548–551, Apr. 2014. doi: 10.1109/LCOMM.2013.123013.132031.
- [26] S. Zhao, Q. Li, Q. Zhang, and J. Qin, "Antenna selection for simultaneous wireless information and power transfer in MIMO systems," *IEEE Communications Letters*, vol. 18, no. 5, pp. 789–792, May 2014. doi: 10.1109/LCOMM.2014.031514.140136.
- [27] X. Zhou, "Training-based swipt: optimal power splitting at the receiver," *IEEE Transactions on Vehicular Technology*, vol. 64, no. 9, pp. 4377–4382, Sept. 2015.
- [28] Z. Zhou, M. Peng, Z. Zhao, W. Wang, and R. S. Blum, "Wireless-powered cooperative communications: power-splitting relaying with energy accumulation," *IEEE Journal on Selected Areas in Communications*, vol. 34, no. 4, pp. 969–982, Apr. 2016.
- [29] S. Y. Lee and C. C. Lai, "A 1-v wideband low-power CMOS active differential power splitter for wireless communication," *IEEE Transactions on Microwave Theory and Techniques*, vol. 55, no. 8, pp. 1593–1600, Aug. 2007. doi: 10.1109/TMTT.2007.901130.
- [30] I.-C. Chang, J.-C. Kao, J.-J. Kuo, and K.-Y. Lin, "An active CMOS one-to-four power splitter for 60-GHz phased-array transmitter," in *2012 IEEE MTT-S International Microwave Symposium (MTT)*, Montreal, Canada, Jun. 2012, pp. 1–3. doi: 10.1109/MWSYM.2012.6258331.
- [31] Y. Dong, M. J. Hossain, and J. Cheng, "Joint power control and time switching for SWIPT systems with heterogeneous QoS requirements," *IEEE Communications Letters*, vol. 20, no. 2, pp. 328–331, Feb. 2016. doi: 10.1109/LCOMM.2015.2498151.
- [32] G. Huang, Q. Zhang, and J. Qin, "Joint time switching and power allocation for multicarrier decode-and-forward relay networks with SWIPT," *IEEE Signal Processing Letters*, vol. 22, no. 12, pp. 2284–2288, Dec. 2015. doi: 10.1109/LSP.2015.2477424.
- [33] F. Khan and Z. Pi, "mmWave mobile broadband (MMB): unleashing the 3–300GHz spectrum," in *34th IEEE Sarnoff Symposium*, Princeton, USA, May 2011, pp. 1–6. doi: 10.1109/SARNOF.2011.5876482.
- [34] J. P. Curty, N. Joehl, F. Krummenacher, C. Dehollain, and M. J. Declercq, "A model for  $\mu$ -power rectifier analysis and design," *IEEE Transactions on Circuits and Systems I: Regular Papers*, vol. 52, no. 12, pp. 2771–2779, Dec. 2005. doi: 10.1109/TCSI.2005.854294.
- [35] G. D. Vita and G. Iannaccone, "Design criteria for the RF section of UHF and microwave passive RFID transponders," *IEEE Transactions on Microwave Theory and Techniques*, vol. 53, no. 9, pp. 2978–2990, Sept. 2005. doi: 10.1109/TMTT.2005.854229.
- [36] Y. Han and D. Perreault, "Analysis and design of high efficiency matching networks," *IEEE Transactions on Power Electronics*, vol. 21, no. 5, pp. 1484–1491, Sept. 2006. doi: 10.1109/TPEL.2006.882083.
- [37] Y. Uzun, "Design and implementation of RF energy harvesting system for low-power electronic devices," *Journal of Electronic Materials*, pp. 1–6, 2016. [Online]. Available: <http://dx.doi.org/10.1007/s11664-016-4441-5>
- [38] M. Pinuela, P. D. Mitcheson, and S. Lucyszyn, "Ambient RF energy harvesting in urban and semi-urban environments," *IEEE Transactions on Microwave Theory and Techniques*, vol. 61, no. 7, pp. 2715–2726, Jul. 2013. doi: 10.1109/TMTT.2013.2262687.
- [39] M. K. Hosain, A. Z. Kouzani, M. F. Samad, and S. J. Tye, "A miniature energy

## Towards Practical Implementation of Data and Energy Integrated Networks

HU Jie, ZHANG Yitian, YU Qin, and YANG Kun

- harvesting rectenna for operating a head-mountable deep brain stimulation device," *IEEE Access*, vol. 3, pp. 223–234, Apr. 2015. doi: 10.1109/ACCESS.2015.2414411.
- [40] Y. Wu, J. P. Linnartz, H. Gao, M. K. Matters-Kammerer, and P. Baltus, "Modeling of RF energy scavenging for batteryless wireless sensors with low input power," in *IEEE 24th Annual International Symposium on Personal, Indoor, and Mobile Radio Communications (PIMRC)*, London, UK, Sept. 2013, pp. 527–531.
- [41] R. E. Barnett, J. Liu, and S. Lazar, "A RF to DC voltage conversion model for multi-stage rectifiers in UHF RFID transponders," *IEEE Journal of Solid-State Circuits*, vol. 44, no. 2, pp. 354–370, Feb. 2009.
- [42] G. Pappotto, F. Carrara, A. Finocchiaro, and G. Palmisano, "A 90-nm CMOS 5-mbps crystal-less RF-powered transceiver for wireless sensor network nodes," *IEEE Journal of Solid-State Circuits*, vol. 49, no. 2, pp. 335–346, Feb. 2014.
- [43] J. Yi, W. H. Ki, and C. Y. Tsui, "Analysis and design strategy of UHF micro-power CMOS rectifiers for micro-sensor and RFID applications," *IEEE Transactions on Circuits and Systems I: Regular Papers*, vol. 54, no. 1, pp. 153–166, Jan. 2007. doi: 10.1109/TCSI.2006.887974.
- [44] A. K. Jonscher, "Energy losses in charging and discharging of capacitors," *IEEE Transactions on Electrical Insulation*, vol. EI-22, no. 4, pp. 361–364, Aug. 1987. doi: 10.1109/TEI.1987.298894.
- [45] H. Yang and Y. Zhang, "Analysis of supercapacitor energy loss for power management in environmentally powered wireless sensor nodes," *IEEE Transactions on Power Electronics*, vol. 28, no. 11, pp. 5391–5403, Nov. 2013. doi: 10.1109/TPEL.2013.2238683.
- [46] R. Chai and Y. Zhang, "A practical supercapacitor model for power management in wireless sensor nodes," *IEEE Transactions on Power Electronics*, vol. 30, no. 12, pp. 6720–6730, Dec. 2015.
- [47] A. Urbina, R. Jungst, D. Ingersoll, et al., "Probabilistic analysis of rechargeable batteries in a photovoltaic power supply system," Sandia National Laboratories, Albuquerque, USA, Tech. Rep. SAND98-2635C, 1988.
- [48] K. Huang and E. Larsson, "Simultaneous information and power transfer for broadband wireless systems," *IEEE Transactions on Signal Processing*, vol. 61, no. 23, pp. 5972–5986, Dec. 2013. doi: 10.1109/TSP.2013.2281026.
- [49] K. Huang, C. Zhong, and G. Zhu, "Some new research trends in wirelessly powered communications," *IEEE Wireless Communications*, vol. 23, no. 2, pp. 19–27, Apr. 2016. doi: 10.1109/MWC.2016.7462481.
- [50] H. Zhai, H. K. Pan, and M. Lu, "A practical wireless charging system based on ultra-wideband retro-reflective beamforming," in *2010 IEEE Antennas and Propagation Society International Symposium*, Toronto, Canada, Jul. 2010, pp. 1–4.
- [51] W. K. G. Seah and J. P. Olds, "Wireless sensor network powered by RF energy harvesting: design and experimentation," Victoria University of Wellington, Wellington 6140, New Zealand, Tech. Rep. ECSTR12-06, Feb. 2012. [Online]. Available: <https://ecs.victoria.ac.nz/foswiki/pub/Main/TechnicalReportSeries/ECSTR12-06.pdf>

Manuscript received: 2016-06-03

## Biographies

**HU Jie** (hujie@uesct.edu.cn) received his BEng and MSc degrees from the School of Information and Communication Engineering, Beijing University of Posts and Telecommunications, China in 2008 and 2011, respectively. He received the PhD degree from the Faculty of Physical Sciences and Engineering, University of Southampton, UK in 2015. Since March 2016, he has been working with the School of Communication and Information Engineering, University of Electronic Science and Technology of China (UESTC), China, as a Lecturer. He has a broad range of interests in wireless communication and networking, such as cognitive radio and cognitive networks, mobile social networks, data and energy integrated networks and tactile Internet.

**ZHANG Yitian** (yzhangbc@essex.ac.uk) received the BEng degree from a joint education of Beijing Institute Technology, China and University of Central Lancashire, UK. He received the MSc degree from Coventry University, UK and he is doing PhD research in University of Essex, UK. His current research interests embrace high efficiency wireless network, Internet of Things and energy harvesting system. He was partly funded by UK EPSRC Project DANCER (EP/K002643/1) in 2015 and he focused his work on energy saving in wireless sensor network. The related work was published on the 14th IEEE International Conference on Ubiquitous Computing and Communications (IUCC-2015).

**YU Qin** (yuqin@uestc.edu.cn) received the BS degree in communication engineering from the Chongqing University of Posts and Telecommunications, China and the MS and PhD degrees in communication and information engineering from UESTC. She conducted postdoctoral research in information security at UESTC from 2007 to 2009. Supported by the Ministry of Education of Chinese Government, she performed visiting research at the Department of Computer Science, Purdue University, USA. She is currently an associate Professor in the School of Communication and Information Engineering of UESTC. She is a member of IEEE, IEEE Communications Society, and Japan IEICE. Her current research interests include wireless networks/communications, data and energy integrated wireless communication networks, and information security. She has published more than 40 papers in the above research areas.

**YANG Kun** (kunyang@essex.ac.uk) received his PhD from the Department of Electronic & Electrical Engineering of University College London (UCL), UK. He is currently a Chair Professor in the School of Computer Science & Electronic Engineering, University of Essex, leading the Network Convergence Laboratory (NCL), UK. He is also an affiliated professor at UESTC. He manages research projects funded by various sources such as UK EPSRC, EU FP7/H2020 and industries. He has published more than 100 journal papers. He serves on the editorial boards of both IEEE and non-IEEE journals. He is a Senior Member of IEEE and a Fellow of IET. His main research interests include wireless networks, future internet technology and network virtualization, and mobile cloud computing and networking.